

INVESTIGATING PETROLOGIC INDICATORS OF MAGMATIC PROCESSES IN VOLCANIC ROCKS

Prevalence of growth twins among anhedral plagioclase microlites†

CARRIE R. BRUGGER<sup>1,\*</sup> AND JULIA E. HAMMER<sup>1</sup>

<sup>1</sup>Department of Geology and Geophysics, University of Hawaii Manoa, Honolulu, Hawaii 96822, U.S.A.

ABSTRACT

Crystal textures of volcanic rocks record the processes involved in magma storage and eruptive ascent. Syn-eruptive crystallization, in which groundmass crystals form and grow according to environmental factors such as thermodynamic undercooling, strongly influences the texture of erupted magma. This stage is difficult to isolate for study in natural rocks, but well-suited for laboratory experiments because the chemical compositions and crystallization timescales of eruptive processes can be emulated. This study examines the incipient stages of plagioclase crystallization in hydrous rhyodacite magma undergoing decompression-driven degassing. Experimental samples in which crystal growth at both near-equilibrium and far-from equilibrium conditions were examined using electron backscatter diffraction (EBSD) analysis to ascertain crystallographic lattice orientations of individual crystals. The crystal orientation investigation affirms a common assumption invoked in textural studies of crystal number density: contiguous crystals with parallel faces are crystallographically continuous, whereas contiguous crystals with non-parallel faces have unrelated crystal lattice orientations and as such, represent separate crystals. In the highly undercooled sample, twinning is identified in ~87% of the crystals examined; in the near-equilibrium sample, 38% of the crystals are twinned. We find that the observed twinning is unlikely to be the result of deformation, transformation, or synneusis, but rather a result of growth defects introduced during the incipient stages of crystallization. We suggest internal structural defects (twins) control macroscopic morphological defects (embayments, swallowtails, and melt inclusions) as a result of the high energy of the twin plane boundary. Formation of twins during the incipient stages of plagioclase crystallization is the single most important factor contributing to anhedral morphologies of feldspar microlites growing during magma decompression, and plays a role in the development of some plagioclase-hosted melt inclusions.

**Keywords:** Electron backscatter diffraction, plagioclase, growth twinning, crystal morphology

INTRODUCTION

Metrics such as crystal sizes, shapes, number densities, and spatial distributions or preferred orientations are used to characterize samples and correlate microtexture with volcanic events (e.g., Cashman 1990, 1992, 1993; Hammer et al. 1999, 2000; Castro et al. 2002; Martel and Poussineau 2007; Genareu et al. 2010). Recent textural studies focus on microlites (crystals <30 μm) to study the details of magma ascent processes (e.g., Geschwind and Rutherford 1995; Hammer et al. 1999; Noguchi et al. 2006, 2008). Microlites that form and grow in highly undercooled environments have characteristic morphologies (hopper, skeletal, dendritic, swallowtailed, and irregular), which may hamper quantitative determination of crystal size and number density because these metrics require unambiguous identification of individual crystals. Distinguishing between impinging crystals and a single crystal with anhedral morphology, for example, can be difficult in an optical photomicrograph or two-

dimensional backscattered electron (BSE) image. Contiguous particles with parallel faces are typically considered to be the anhedral continuations of one crystal and are thus counted as a single grain. In contrast, touching grains with non-parallel faces are considered and counted as separate grains (e.g., Pupier et al. 2008; Brugger and Hammer 2010b). Although widely applied (cf. Hammer et al. 1999), this criterion for crystal recognition in textural studies has never been corroborated by independent assessment of the crystallographic lattice orientations of grains. Electron backscatter diffraction (EBSD) allows evaluation of this assumption. Using a standard petrographic thin section and SEM, it is possible to map in situ the three-dimensional crystallographic orientations of minerals or portions of minerals as small as 0.5 μm and reliably identify small angular variations in the lattice orientation of adjacent grains or subgrain regions (Prior et al. 1999, 2009). Thus the EBSD technique adds crystallographic orientation characterization to the set of techniques that may be routinely used to investigate microlite textures.

In this study we examine the crystallographic structure and orientation of plagioclase microlites in two experimental samples that formed under known conditions of thermodynamic undercooling with the goal of understanding the early development of crystal morphologies commonly encountered in igneous rocks. Our specific objectives are twofold: (1) to critically evaluate the

\* Present address: School of Earth Sciences and Environmental Sustainability, Northern Arizona University, Flagstaff, Arizona 86011, U.S.A. E-mail: carrie.brugger@nau.edu

† Special collection papers can be found on GSW at <http://ammin.geoscienceworld.org/site/misc/specialissueulist.xhtml>.

assumption that contiguous crystals with non-parallel faces are separate crystals, and (2) to examine the relationship between internal crystallographic structure and external morphologies, and evaluate whether anhedral crystals exhibit a higher incidence of internal defects (such as subgrain lattice misorientations) than do euhedral crystals (e.g., Welsch et al. 2013).

## METHOD

### Sample selection

This study utilizes two samples, both of which were experimental runs from the suite described in full by Brugger and Hammer (2010a). Each sample has the same bulk composition, rhyodacite from the 3430 yBP eruption of Aniakchak Volcano in Alaska, and each experiment was saturated with an H<sub>2</sub>O-rich fluid. The first sample (1-3) represents near-equilibrium conditions. This sample was held for 25 h at the pre-eruptive storage conditions of this rhyodacite magma, 880 °C and 130 MPa, as determined by Larsen (2006). All of the crystals in this higher pressure sample are euhedral and characterized by faceted, convex morphologies. The second sample (15-4) was decompressed from 130 to 5 MPa at a rate of 1 MPa/h and quenched immediately upon reaching 5 MPa. Comparisons of plagioclase crystal content and glass chemistry between this sample and long duration dwell experiments at four pressures between 87 and 5 MPa indicate an increasing degree of undercooling during decompression [cf. Figs. 5 and 7 in Brugger and Hammer (2010a)]. Thus, this sample represents a highly undercooled melt with a population of rapidly formed plagioclase crystals (Brugger and Hammer 2010a). Euhedral laths are rare in this sample. Most grains have anhedral morphologies: irregular faces with irregular indentations, hopper cavities, or swallowtail morphologies. Melt inclusions are also common in these crystals.

### EBSD analysis

Chips from each experimental sample were mounted to thin section slides, then ground and polished to a finish appropriate for microprobe analysis following standard abrasion techniques. Samples were then subjected to a three-hour final treatment on a Buehler VibroMet 2 Vibratory Polisher using Buehler Mastermet 2, a non-crystallizing colloidal silica polishing suspension. No electrically conductive coating was applied to the samples as this interferes with the acquisition of backscattered electron diffraction patterns (EBSPs). After the target crystals were mapped with EBSD, a carbon coat was applied to the surface and BSE (backscatter electron) images of the crystals were acquired.

Electron backscatter diffraction (EBSD) maps (e.g., Fig. 1) were generated on the JEOL 5900LV scanning electron microscope (SEM) at the University of Hawaii Manoa utilizing a Nordlys Detector and the HKL CHANNEL5 acquisition software Flamenco from Oxford Instruments (using specific operating conditions detailed in the Appendix<sup>1</sup>). To prevent electrical charging on the sample surface the SEM was operated at low vacuum (15 Pa).

In the low-undercooling, higher pressure sample, the crystals mapped with EBSD ranged in size from 40–340 μm in length; mapped crystals in the lower pressure sample were 20–120 μm long. Due to the small size of crystals and the relative abundance of glass and vesicles between grains, separate maps were created for individual feldspar crystals or groups of crystals rather than mapping the entire sample. Because small areas of the sample were mapped individually, it was not necessary to apply a correction factor to minimize distortion away from the image center. Mapped areas ranged in size from 24 × 16 μm up to 176 × 288 μm, and the step size between each analysis ranged from 1–10 μm, depending on the size of the target crystal. In some cases the entire crystal was not mapped, corners or edges of crystals were omitted in some maps in the interest of saving time during mapping and indexing.

Because of the poor pattern quality associated with low-symmetry crystals, we used a combination of manual and automated indexing techniques in our plagioclase analyses. After each map was completed and all EBSPs saved, the first few rows of electron backscatter patterns (EBSP) were manually indexed to optimize the indexing conditions (number of bands, Hough resolution, and band centers or edges; Appendix<sup>1</sup>). Once optimized, the remaining EBSPs in each EBSD map underwent automated indexing using the Flamenco software

from HKL Technology. All samples were indexed with the same “anorthite” match unit from the *American Mineralogist* Crystal Structure Database (Angel et al. 1990) where  $a = 8.1796 \text{ \AA}$ ,  $b = 12.8747 \text{ \AA}$ ,  $c = 14.1720 \text{ \AA}$ ,  $\alpha = 93.13^\circ$ ,  $\beta = 115.89^\circ$ ,  $\gamma = 91.24^\circ$ , and space group  $P\bar{1}$ . Indexed patterns with mean angular deviation (MAD) values  $<1.1^\circ$  were discarded, although average MAD values were much lower, closer to 0.3–0.7. During a post-processing noise reduction step, all isolated map pixels (EBSPs) with an indexed orientation different from the eight surrounding EBSPs, were removed from the map. If the pixel was surrounded by at least six neighboring pixels with the same orientation, then EBSP was changed to match the surrounding values. If less than six of the neighboring pixels were the same, then the isolated pixel was changed to a zero solution, which appears black in the EBSD maps.

For each electron backscatter diffraction map, pole figures were generated with the HKL CHANNEL 5 module Mambo. Angular relationships between corresponding crystallographic axes in neighboring crystals, or across twin boundaries within crystals, were assessed manually using the measurement tool (e.g., Fig. 1). Replicate measurements of the same pair of poles indicate measurement errors on the order of ~1–8°.

### Twinning

The low (triclinic) symmetry of plagioclase means that twin operators are limited to 180° rotations about one of the crystallographic axes, or reflections across crystal faces (Smith and Brown 1988). Each of the recognized feldspar twin relationships (e.g., Deer et al. 1992; page 407) were simulated using SHAPE (version 7.2.3) software (Dowty 1980a, 2008) and the  $a$ ,  $b$ , and  $c$  crystallographic axial lengths and the  $\alpha$ ,  $\beta$ , and  $\gamma$  angular relationships for the plagioclase match unit (see above) used in indexing (Fig. 2). In addition, the angular relationships between corresponding crystallographic axes (e.g.,  $a^*a$ ) were determined for each twin law (Fig. 2) by visual examination. Crystal twinning was identified in samples by comparing the angular relationships measured in the CHANNEL 5 pole figure module, Mambo (Fig. 1), with expected twin relationships determined using SHAPE.

## RESULTS

EBSB orientation maps were generated for 16 plagioclase crystals in the higher pressure (130 MPa) sample and 79 crystals in the lower pressure (5 MPa) sample. The higher pressure sample crystallized at conditions near the liquidus and contains very few crystals, thus all plagioclase crystals longer than 20 μm in the thin section were mapped. The lower pressure sample contains significantly more crystals, thus the mapped crystals represent ~35% of all plagioclase crystals  $\geq 20 \mu\text{m}$  in length in this sample.

EBSB mapping reveals random single-pixel variations in crystallographic orientation ( $<5^\circ$ ) across individual grains that likely correspond to slight differences in EBSP indexing rather than genuine variations in crystallographic orientation (Prior et al. 1999). Mapping also exposes abundant twinning according to common plagioclase twin laws (Fig. 2), as described in more detail below. Previous studies of dendritic crystal morphologies formed by diffusion-limited growth in igneous environments report incremental, progressive rotations of the crystal lattices of clinopyroxene within grains and subgrain boundaries (Hammer et al. 2010; Welsch et al. 2013), however, this study found no such small-angle subgrain lattice misorientations in plagioclase.

### Crystallographic relationships between contiguous plagioclase crystals

A total of 35 pairs of contiguous plagioclase crystals with non-parallel faces were examined in the lower pressure sample (e.g., Fig. 3a; Table 1); there were no touching crystals to investigate in the higher pressure sample. EBSD orientation mapping reveals that touching crystals with non-parallel faces are unrelated by any twin law (e.g., Fig. 3a). In contrast, all

<sup>1</sup> Deposit item AM-15-24809, Appendix. Deposit items are stored on the MSA web site and available via the *American Mineralogist* Table of Contents. Find the article in the table of contents at GSW (ammin.geoscienceworld.org) or MSA (www.minsocam.org), and then click on the deposit link.

mapped contiguous crystals with parallel faces (e.g., Fig. 3b) are related by twin laws.

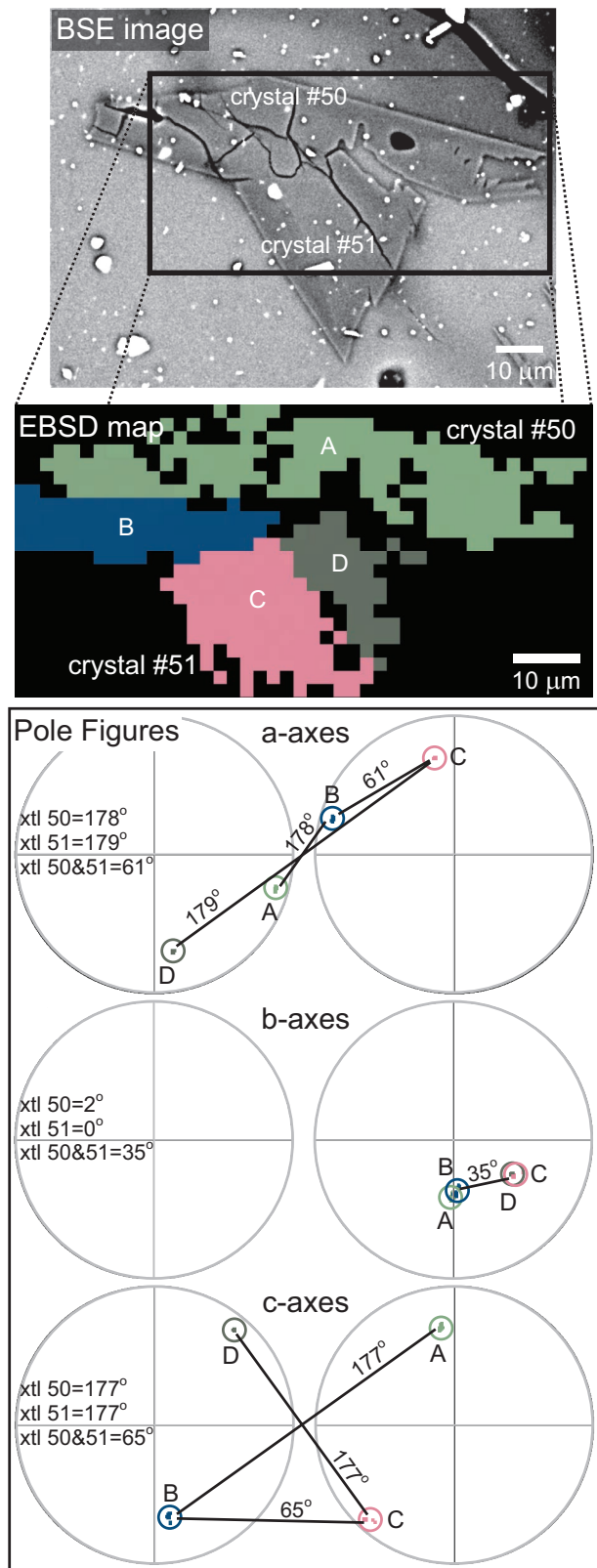
### Twinning

**Near-equilibrium sample.** In the higher pressure sample, 10 (63%) of the 16 mapped crystals contain no twinning. Of the six crystals that are twinned, five display Pericline twinning and one crystal is twinned according to the Ala twin law (Tables 2 and 3; Fig. 2). Half of the twinned crystals display simple twins, while three of the crystals with pericline twinning contain multiple twins, or two to four alternations in crystallographic orientation across the exposed crystal section plane.

**Highly undercooled sample.** Of the 79 mapped crystals in the lower pressure sample, only 10 crystals (13%) are untwinned. Of the 69 crystals that are twinned, 49 display only one type of twinning and 20 contain more than one type (Table 2). Pericline and Carlsbad twins are the two most commonly observed twin laws, with 50 and 21 examples of each, respectively (Table 3). There are also 19 examples of twinning that involve a compound Pericline-Carlsbad twin. In addition, two crystals contain Ala twins and one crystal has a combination Ala-Pericline twin. In natural plagioclase crystals, polysynthetic Albite and Pericline twinning is common (Smith and Brown 1988). However, in these experimentally produced crystals, no polysynthetic twinning is observable at the resolution of the EBSD mapping. Nearly all the observed twins are simple twins, although nine crystals contain multiple twins, which consist of two to three changes in orientation across the crystal section. The twin planes are commonly parallel to the crystal faces. Many crystals display morphological “defects” such as hopper cavities, melt inclusions, embayments, swallowtails, and uneven terminations. Some melt inclusions are enclosed in a crystallographically homogeneous host (Fig. 4a), but the vast majority of morphological defects lie along twin boundaries (Figs. 4b–4f).

In summary, twinning is approximately twice as common in the lower pressure sample (15-4) than the higher pressure sample (1-3). Because sample 15-4 was annealed at the same pressure and temperature conditions as sample 1-3 prior to the commencement of decompression, the increase in twinning frequency must result from crystals that formed and grew during the decompression of sample 15-4.

► **FIGURE 1.** Examples of pole figures generated by CHANNEL 5 Mambo software, along with corresponding EBSD orientation map and BSE image. Each color (also labeled with a capital letter) in the EBSD map represents a different crystallographic orientation, which is keyed to the corresponding colored pixels in the pole figures (also labeled with the corresponding letter). Within each colored region on the EBSD map there are slight variations in orientation, thus pole figures contain clusters of dots (circled) rather than a single point. Each pair of pole figures represents the upper (left) and lower (right) hemisphere for the *a*-axes (top), *b*-axes (middle), and *c*-axes (bottom). Because plagioclase is triclinic, there is only one pole for each crystallographic direction (i.e., the upper and lower hemispherical projections are distinct). Angular relationships between poles is assessed with the measurement tool in the program Mambo (represented by black lines connecting clusters of dots). The relationship between the two shaded regions of crystal 51 (labeled C and D) is: *a*-axis = 179°, *b*-axis = 0°, *c*-axis = 177°, which represents a pericline twin relationship. The same angular relationship exists between the two regions (labeled A and B) of crystal 50. However, there is no twin relationship that matches the angular relationships between crystal 50 and crystal 51.



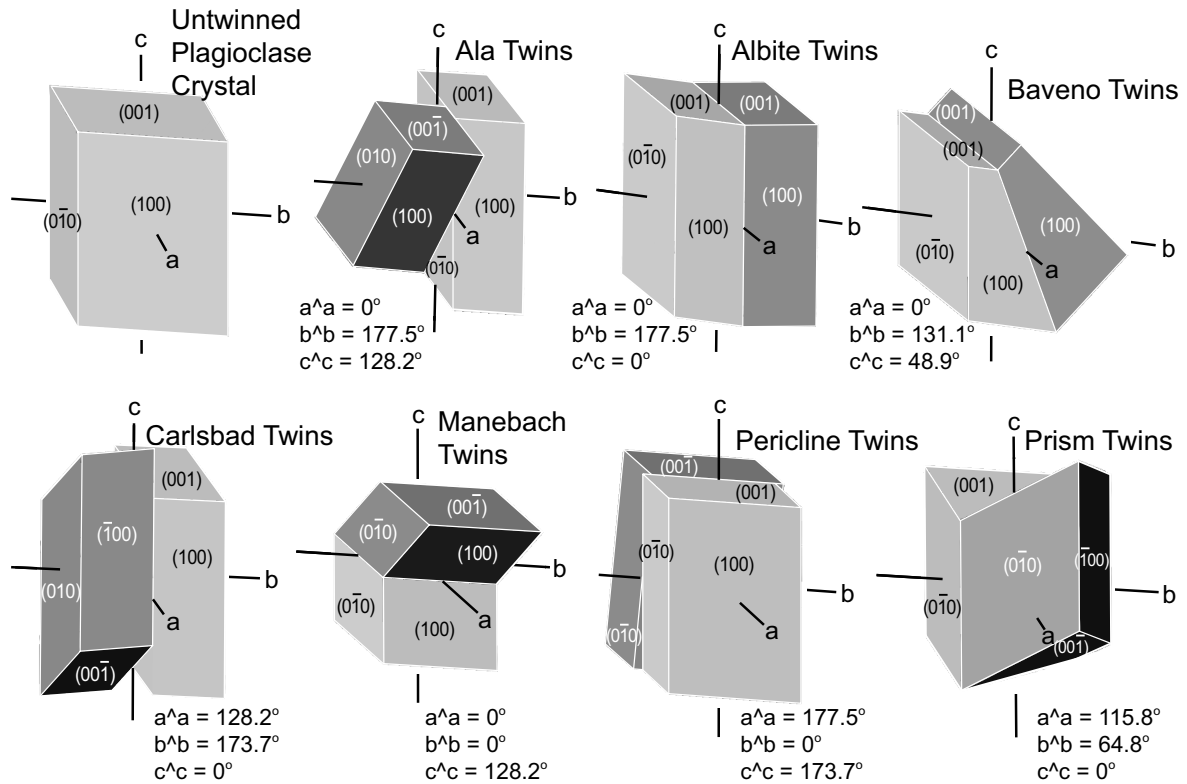


**FIGURE 2.** Examples of some of the most common twin laws examined using SHAPE software and the resulting angular relationships between the crystallographic axes of twinned crystals. The lighter colored crystal in each twin represents the original crystal and it is in approximately the same orientation in each example (the  $a$ -,  $b$ -, and  $c$ -crystallographic axes shown correspond to the original crystal only). The darker colored crystal represents the twin that results from the given twin law. Visible crystal faces are labeled with the appropriate Miller indices. Given the two-dimensional slices and anhedral morphologies, these particular habits are not likely to be realized in the BSE images. For clarity, only the  $\{100\}$ ,  $\{010\}$ , and  $\{001\}$  crystal forms for the specific plagioclase match unit used in this study are shown.

## DISCUSSION

### Causes of twinning

Twinning in plagioclase may result from deformation, transformation, or growth (Buerger 1945). Carlsbad, Manebach, and Baveno twins are produced only by growth, whereas Pericline and Albite twins can be produced by deformation, transformation, or growth (Smith and Brown 1988). For the reasons outlined below, we conclude that all twinned crystals in the samples of this study are examples of growth twins. Furthermore, energetic considerations explain the prevalence of twinned crystals in the lower pressure sample and relative scarcity in the higher pressure sample.

Mechanical twinning, also known as deformation or glide twinning, is the result of applied shearing stress (Buerger 1945) or an external force applied from a preferred direction (Sunagawa 2005). This stress can result from regional deformation of the rock or by impingement of growth in a crystal mush (Smith and Brown 1988). For plagioclase crystals with intermediate compositions such as our samples ( $An_{24-33}$ ), production of mechanical twins requires a high level of stress at elevated temperatures to create high-energy twin boundaries (Borg and Handin 1966; Borg and Heard 1969; Punin et al. 2009). However, neither of

our samples exceeds 20% crystallinity or displays significant crystal impingement. Thus interference of neighboring crystals is not a probable cause of twin formation. Plagioclase crystals in this study grew at elevated pressure (5–130 MPa) during the experiments; however, the external applied stress was equal in all directions (hydrostatic) and thus incapable of producing differential strain. We conclude that mechanical twinning is not a likely cause of the twinning in these samples.

Transformation twinning is the result of structural changes that occur when a crystal changes symmetry (Smith and Brown 1988). A well-known example of this is the conversion of monoclinic high albite to triclinic low albite during cooling. Smith (1974b) suggests that natural plagioclase never displays transformation twinning because plagioclase in volcanic rocks contains at least 10% calcium and/or potassium and thus never crystallizes with monoclinic symmetry. Pure albite ( $Ab_{100}$ ) converts from monoclinic to triclinic symmetry at  $980^{\circ}\text{C}$ , and the temperature of this conversion increases as the amount of anorthite ( $An$ ) and/or orthoclase ( $Or$ ) increases (Smith 1974a). For the narrow range of plagioclase compositions found in these samples ( $Or_{2.2}Ab_{65}An_{32.8}$  to  $Or_{3.3}Ab_{72.4}An_{24.3}$ ; Brugger and Hammer 2010a), the monoclinic-triclinic inversion occurs at temperatures above  $1100^{\circ}\text{C}$  at one atmosphere pressure (Fig.

7-60 in Smith 1974a). At the higher pressures (5–130 MPa) used during the synthesis of these crystals, this inversion temperature is expected to be even higher. The experiments were conducted at a constant temperature of 880 °C, and thus significantly below the inversion temperature at all pressures studied. Therefore, the crystals in these samples probably formed initially with triclinic symmetry, thus obviating the possibility that twinning was caused

by monoclinic-triclinic inversion.

Growth twinning is caused by an accidental, yet non-random, misalignment of atoms attaching to a crystalline substrate during growth. Formative and recent work suggests this type of twinning typically begins early in the growth history, especially under conditions of supersaturation (Buerger 1945; Nespolo and Ferraris 2004; Sunagawa 2005). During crystal growth, when a

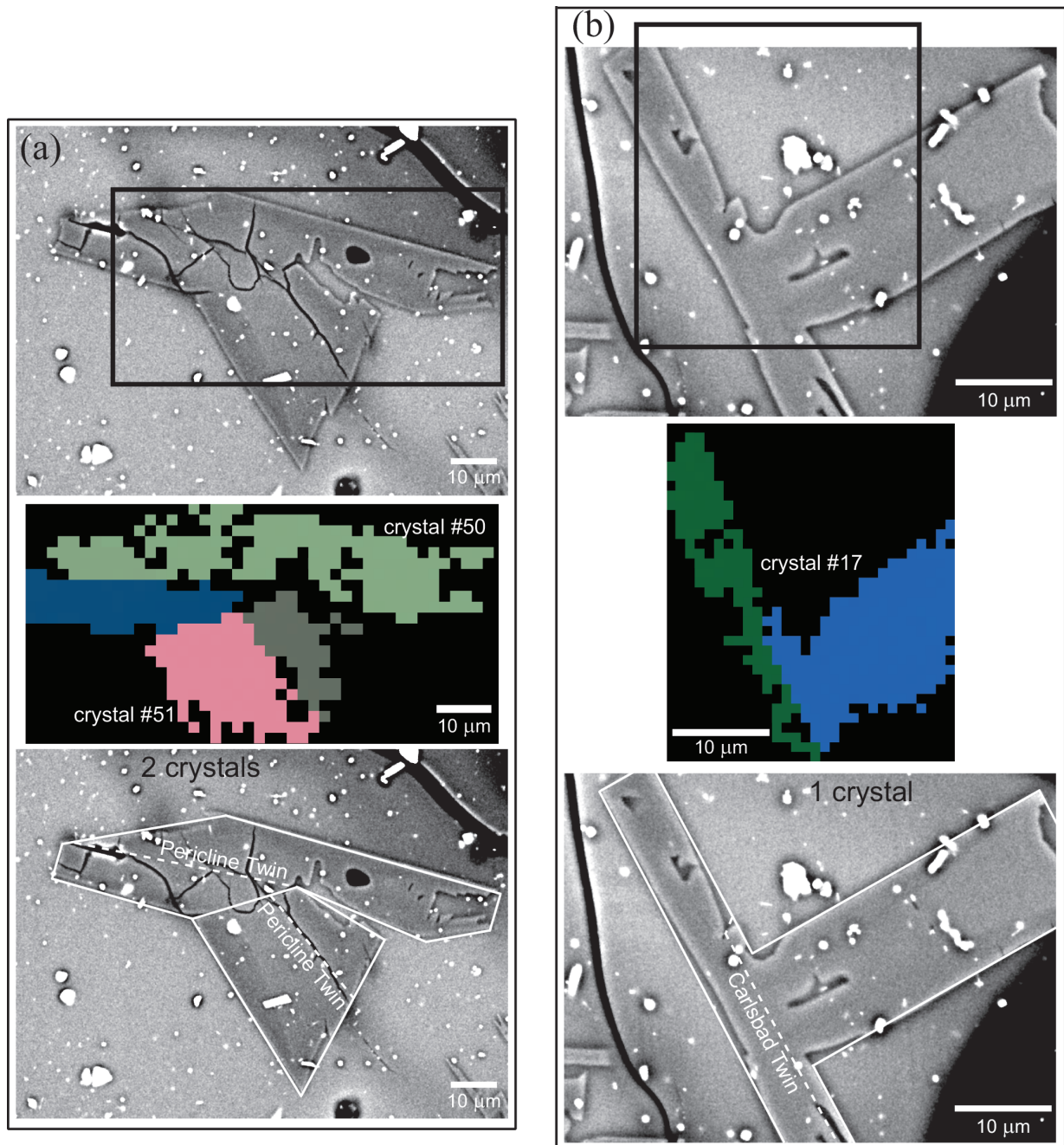


**FIGURE 3.** (a) Example of two contiguous crystals unrelated by a twin law, but each twinned internally. (b) Example of one twinned crystal that may appear to be two contiguous laths at a 90° angle. (top) BSE images with black boxes representing the area mapped by EBSD. (middle) EBSD maps, each color represents a different crystallographic orientation. The map on the left has a step size of 2 mm; the map on the right has a step size of 1 mm. The crystal numbers correspond to the numbers used in Tables 1 and 2. (bottom) Interpretation of the crystal(s) based on the EBSD map. Solid white lines outline each crystal; dashed white lines delineate twin boundaries.

**TABLE 1.** Angular relationships between corresponding axes in contiguous non-related crystals in sample 15-4

Crystal numbers <sup>a</sup>	<i>a</i> -axis <sup>b</sup>	<i>b</i> -axis <sup>b</sup>	<i>c</i> -axis <sup>b</sup>
1	2	19	30
6	7	89	107
6	8	100	120
9	–	50	8
10	11	18	25
11	12	30	160
15	16	25	40
18	19	52	110
20	21	84	99
26	30	13	164
27	75	56	152
27	28	3	131
27	29	43	168
27	30	58	153
30	76	64	165
31	32	22	33
35	36	64	52
36	37	8	32
38	39	4	61
40	41	88	55
42	43	151	28
42	73	134	121
43	73	115	73
44	–	8	22
45	–	9	25
47	48	77	122
49	72	81	147
50	51	61	35
54	55	16	125
58	–	135	70
61	70	153	148
61	62	37	39
64	65	31	43
66	67	25	55
67	68	44	18
			44

<sup>a</sup> Mapped crystals were each assigned a unique number. Occasionally, when only a small portion of an adjacent crystal was mapped, it was not assigned a number and was not included as one of the 79 mapped crystals in this study.

<sup>b</sup> Replicate measurements of the same pair of poles indicate measurement errors on the order of ~1–8°.

new atom or cluster of atoms is added to the crystal face it takes a position that maximizes its coordination with the preexisting atoms and minimizes the surficial free energy of that crystal. However, as the rate of attachment increases, the probability of growth errors increases. Attachment errors during rapid crystal growth arising from high supersaturation is deemed the most likely cause of twinning in the lower pressure sample.

### Crystal growth and twin formation

#### Energetics of attachment at low effective undercooling.

Kinetic theory suggests that when a natural magmatic melt is held at near equilibrium conditions, such as for sample 1-3, a low effective undercooling provides a small driving force for crystallization (Kirkpatrick 1975; Porter and Easterling 1997). Plagioclase components in the melt have the potential to occupy a lower energy state if they attach to the crystal. Once they attach, the resulting change in melt composition may be sufficient to bring the system to equilibrium. If chemical equilibrium is reached, the net attachment of additional crystal components is negligible unless another perturbation in the system (i.e., a drop in temperature or pressure in a water-saturated melt) produces a driving force for crystallization. This idealized case results in a relatively slow rate of attachment, a correspondingly slow crystal growth rate, and the formation of planar crystal faces and euhedral crystals.

If a feldspar unit attaches to the crystal surface in a position that does not continue the normal crystal lattice, it will occupy a subminimal energy state. Under near-equilibrium conditions, this subminimal energy state may actually require higher energy than a return to the liquid state. In this case, there will be a high probability for random fluctuations to cause the unit to detach and then reattach in a lower energy position (Buerger 1945). Thus, at near-equilibrium conditions, the likelihood of growth defects persisting in the crystal structure is quite low. Since growth twinning is an example of such a defect, it follows that crystal growth at low effective undercooling should rarely result in the formation of twinned crystals, which is consistent with the results of this study (Table 3).

#### Energetics of attachment at high effective undercooling.

A magmatic melt far from equilibrium, such as sample 15-4, has a high effective undercooling and a high driving force for crystallization. At high effective undercooling the difference in energy between the melt and the crystal is much greater, and feldspar units attach to the crystal face more rapidly (Porter and Easterling 1997). Under these conditions, the probability of twin formation increases because there is a higher probability of attachment errors, and also because feldspar units that adhere to the crystal face in positions of subminimal energy are more likely to remain attached (Buerger 1945; Cahn 1954). Although they do not occupy the lowest possible energy state, these units are in a lower energy position attached to the crystal than they would be in the melt (Smith and Brown 1988; Sunagawa 2005). The higher energy state of the twin compared to the single crystal is offset by the higher driving force of crystallization under high-supersaturation conditions (Sunagawa 2005). In addition, the rapid movement of additional atoms to the crystal-melt interface may lead to the simultaneous arrival of additional atoms that will improve the coordination and lower the energy of the first misplaced atom, thus increasing the likelihood that a twin persists (Buerger 1945; Nespolo and Ferraris 2004).

Another factor that may contribute to the formation of twins at high effective undercooling is the structure of the melt itself. Classical nucleation theory suggests that highly undercooled melts contain more clusters of atoms having properties of the bulk crystal than do melts near equilibrium, and each cluster is composed of a larger number of attachment units (Porter and Easterling 1997; Kelton 2004). Thus, if a cluster of atoms in an undercooled melt arrives at the crystal surface in a twin position, the twin is more likely to persist because the arriving atoms are already coordinated with one another (Buerger 1945).

The formation of growth twins is most likely to occur during the earliest stages of crystallization (Buerger 1945; Cahn 1954; Smith and Brown 1988; Sunagawa 2005), before development of a spatially extensive substrate to act as a template for new atoms. Small particles have high surface area to volume ratios, and thus high interfacial free energies (e.g., Gibbs-Thomson effect; Porter and Easterling 1992). A twin position provides an attachment configuration for arriving clusters that is intermediate between the energy of an epitaxial and random orientation. If a melt reaches and maintains near-equilibrium conditions soon after the nucleation stage, a small twinned crystal with higher energy may dissolve and then reprecipitate on an untwinned crystal (Cahn 1954). However, if the melt continues crystallizing

**TABLE 2.** Angular relationships between corresponding axes across twin planes

Sample	Crystal number <sup>a</sup>	Type of twin	a-axes <sup>b</sup>	b-axes <sup>b</sup>	c-axes <sup>b</sup>	Simple or multiple twin
1-3	2	pericline twin	179	7	176	simple
1-3	7	Ala twin	0	179	127	simple
1-3	8	pericline twin	179	7	179	multiple
1-3	9	pericline twin	179	7	180	multiple
1-3	10	pericline twin	179	8	178	multiple
1-3	12	pericline twin	178	5	179	simple
15-4	1	carlsbad twin	129	175	0	simple
15-4	2	pericline + carlsbad	52	179	179	multiple
15-4	2	pericline twin	178	7	179	simple
15-4	3	pericline twin	179	2	178	simple
15-4	4	pericline + carlsbad	50	180	180	simple
15-4	4	pericline twin	180	6	180	simple
15-4	4	carlsbad twin	130	174	0	simple
15-4	5	Ala twin	0	180	130	multiple
15-4	6	pericline twin	178	8	179	simple
15-4	6	carlsbad twin	129	174	0	simple
15-4	7	pericline twin	179	7	177	simple
15-4	8	pericline + carlsbad	52	177	178	simple
15-4	8	pericline twin	179	5	178	simple
15-4	9	carlsbad twin	130	180	0	simple
15-4	9	pericline twin	180	3	180	simple
15-4	10	carlsbad twin	129	178	0	simple
15-4	10	pericline twin	179	7	177	simple
15-4	11	pericline + carlsbad	52	175	176	simple
15-4	12	pericline twin	179	4	179	simple
15-4	13	pericline twin	178	0	178	multiple
15-4	14	pericline twin	178	5	178	simple
15-4	14	carlsbad twin	128	175	0	simple
15-4	15	pericline + carlsbad	51	178	179	simple
15-4	16	pericline + carlsbad	51	176	179	simple
15-4	17	carlsbad twin	130	175	0	simple
15-4	18	carlsbad twin	130	175	0	simple
15-4	19	pericline twin	179	3	180	simple
15-4	20	pericline twin	179	5	178	simple
15-4	21	pericline twin	178	8	179	simple
15-4	22	pericline + carlsbad	51	168	180	simple
15-4	22	pericline twin	178	7	178	simple
15-4	23	pericline twin	180	3	180	simple
15-4	24	pericline twin	180	2	180	simple
15-4	25	pericline twin	179	0	178	simple
15-4	26	pericline + carlsbad	51	178	178	simple
15-4	27	pericline twin	178	5	179	simple
15-4	27	carlsbad twin	129	175	0	simple
15-4	28	pericline twin	178	2	176	simple
15-4	28	carlsbad twin	127	174	0	simple
15-4	29	carlsbad twin	128	174	0	simple
15-4	30	pericline + carlsbad	50	176	179	simple
15-4	31	carlsbad twin	131	175	0	simple
15-4	32	pericline + carlsbad	51	176	179	simple
15-4	32	pericline twin	179	7	179	simple
15-4	33	pericline twin	178	6	180	simple

**TABLE 2.—CONTINUED**

Sample	Crystal number <sup>a</sup>	Type of twin	a-axes <sup>b</sup>	b-axes <sup>b</sup>	c-axes <sup>b</sup>	Simple or multiple twin
15-4	34	pericline twin	179	6	179	multiple
15-4	35	carlsbad twin	128	173	0	simple
15-4	36	carlsbad twin	130	174	0	simple
15-4	37	carlsbad twin	130	174	0	simple
15-4	38	pericline twin	178	6	179	simple
15-4	39	pericline twin	178	7	179	simple
15-4	40	pericline twin	179	4	179	simple
15-4	40	carlsbad twin	129	174	0	simple
15-4	41	pericline twin	180	2	178	simple
15-4	41	carlsbad twin	128	179	2	simple
15-4	42	pericline twin	178	2	178	simple
15-4	43	pericline twin	179	7	179	simple
15-4	43	Ala twin	0	178	127	simple
15-4	44	pericline twin	179	0	173	simple
15-4	45	Ala + Pericline	179	179	51	simple
15-4	45	pericline twin	177	0	176	simple
15-4	46	pericline twin	178	0	178	simple
15-4	47	pericline twin	177	6	180	simple
15-4	47	pericline + carlsbad	52	176	180	simple
15-4	48	pericline twin	178	7	179	simple
15-4	49	pericline + carlsbad	51	178	180	simple
15-4	50	pericline twin	178	2	177	simple
15-4	51	pericline twin	179	0	177	simple
15-4	52	pericline twin	179	4	179	simple
15-4	52	carlsbad twin	130	174	0	simple
15-4	52	pericline + carlsbad	51	176	179	simple
15-4	53	pericline twin	179	0	175	simple
15-4	54	carlsbad twin	128	173	0	simple
15-4	55	pericline twin	179	7	180	simple
15-4	56	pericline + carlsbad	51	175	180	simple
15-4	56	pericline twin	179	8	180	simple
15-4	56	pericline twin	178	7	180	simple
15-4	57	pericline twin	178	6	179	multiple
15-4	58	pericline + carlsbad	52	175	179	simple
15-4	58	pericline twin	178	8	179	simple
15-4	59	pericline twin	178	8	178	multiple
15-4	60	pericline twin	178	6	179	simple
15-4	61	carlsbad twin	128	175	0	simple
15-4	62	carlsbad twin	128	173	0	simple
15-4	62	pericline twin	176	5	178	simple
15-4	62	pericline + carlsbad	51	179	179	simple
15-4	63	pericline twin	178	8	177	multiple
15-4	64	pericline + carlsbad	51	175	180	simple
15-4	65	pericline + carlsbad	51	174	180	simple
15-4	66	pericline + carlsbad	51	177	178	simple
15-4	67	pericline twin	177	7	179	simple
15-4	68	pericline twin	178	0	174	multiple
15-4	69	pericline twin	179	9	179	simple

<sup>a</sup> Crystals that appear more than once in this list exhibit multiple types of twins across different subgrain boundaries.

<sup>b</sup> Replicate measurements of the same pair of poles indicate measurement errors on the order of ~1–8°.

**TABLE 3.** Frequency and type of twinning found in each sample

Sample	n <sup>a</sup>	Total twinned crystals	Ala twin	Pericline twin	Carlsbad twin	Pericline + Carlsbad	Pericline + Ala
1-3	16	6	1	5	0	0	0
15-4	79	69	2	50	21	19	1

<sup>a</sup> Total number of mapped crystals.

under conditions of supersaturation, as experienced by sample 15-4 during continuous decompression (Brugger and Hammer 2010a), then continued growth of the twin will occur (Emmons and Gates 1943; Buerger 1945). In fact, twinned nuclei have been observed to grow faster than single crystal nuclei once they are established (Cahn 1954).

Growth twinning as a result of supersaturation occasionally reoccurs, as evidenced by the presence of some crystals with multiple twin planes. However, the vast majority of crystals in our samples contain simple twins approximately equal in size,

which likely formed as the result of an error during the earliest stages of crystal growth. Polysynthetic twinning is not present in any of our samples. This is in agreement with previous research (Emmons and Gates 1943; Cahn 1954) that suggests polysynthetic twinning is not produced during growth, but rather by sub-solidus structural inversion during cooling late in the growth history or by mechanical deformation resulting from external forces or internal crystal impingement forces.

**Synneusis.** Synneusis refers to the “swimming together” of crystals (Vogt 1921). In the context of twinning, it has been

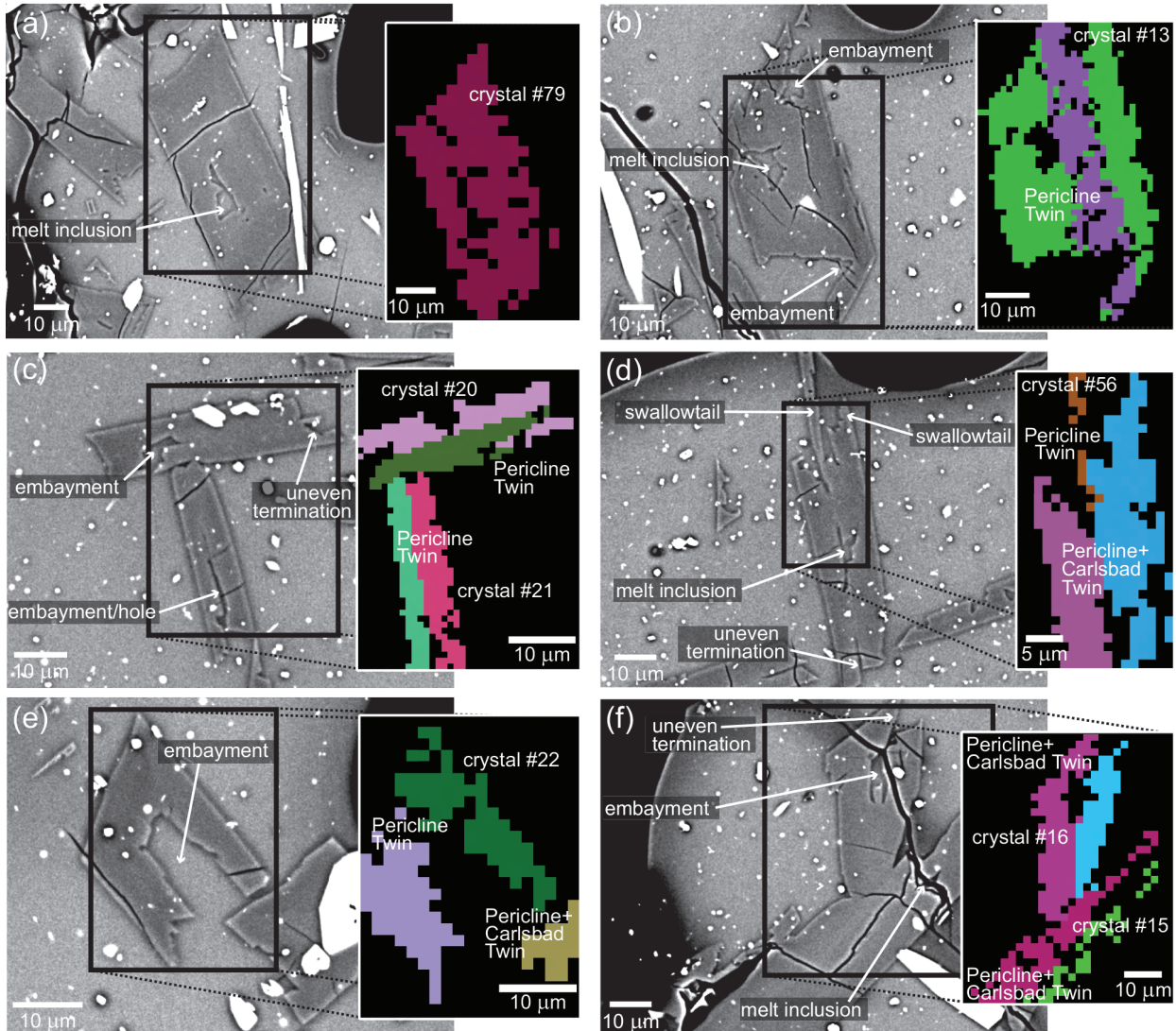


**FIGURE 4.** BSE images and corresponding EBSD maps for select grains in sample 15-4. Black boxes in BSE images correspond to the area mapped in the EBSD images. Each color in the EBSD maps represents a different crystallographic orientation. The crystal numbers correspond to the numbers used in Tables 1 and 2. (a) Morphological defects entirely within one crystallographic orientation are rare. (b–f) Morphological defects (embayments, swallowtails, uneven terminations, and melt inclusions) usually lie along twin boundaries, as shown in these images.

described as a process by which two crystals suspended in a melt may float together and attach along external faces to create a simple twin joined by any number of different twin laws (Vance 1969; Smith and Brown 1988; Nespolo and Ferraris 2004). For this process to occur, the crystals must be in an environment that favors their motion and casual interaction so that they may come into random contact (Nespolo and Ferraris 2004) and, when necessary, rotate into structural alignment (Cahn 1954; Spiess et al. 2001; Ikeda et al. 2002; Ohfuji et al. 2005). Some authors consider synnesis a sub-type of growth twinning (e.g., Smith 1974b; Punin et al. 2009) although it occurs once the crystals are of observable size (Vance 1969). We consider growth twinning to involve errors in the attachment of molecular-scale feldspar growth units to a crystal face, and thus consider synnesis here

as a separate potential mechanism of twin formation.

Synnesis is invoked to explain crystal clustering in a wide variety of analog and natural systems. It is observed in situ in laboratory experiments of plagioclase crystals suspended in heavy liquids (Viola 1902), as well as in saturated solutions of lead nitrate, lithium sulfate, alum and cadmium iodide (Gaubert 1896; Johnsen 1907; Schaskolsky and Schubnikow 1933; Kitazawa et al. 1971). Notably, synnesis is observed when relatively low viscosity solutions are shaken, stirred, or otherwise mechanically agitated. When the same liquids are left to crystallize undisturbed, synnesis is less common or does not occur at all. Synnesis has been proposed for natural magmas as well. Based on evidence from zoning patterns and/or blocky crystal outlines, synnesis has been inferred for glomeroporphy-

ritic aggregates of plagioclase, quartz, and chromite in natural volcanic and plutonic rocks ranging in composition from dunite to granodiorite (Vogt 1921; Ross 1957; Vance and Gilreath 1967; Vance 1969). Olivine crystal aggregates from Kilauea Iki are also suggested as synneusis candidates (Schwindinger and Anderson 1989), although other explanations are also plausible (Welsch et al. 2013). Finally, synneusis is proposed to explain decreases in plagioclase and olivine crystal number densities in basaltic magmas even without visual evidence that this process occurred (Higgins and Chandrasekharam 2007; Pupier et al. 2008; Vinet and Higgins 2010).

Because synneusis cannot be explicitly determined by examining final crystal textures (Dowty 1980b), unequivocal verification of synneusis requires *in situ* observations during crystallization. The first *in situ* observations of plagioclase synneusis in basaltic-andesite melt are reported for experiments at 900 °C and 1 bar pressure (Schiavi et al. 2009). At present there is no technology available that allows surveillance of crystal growth at elevated pressure (Hammer 2009), and thus we cannot eliminate the possibility that synneusis occurs in our experiments. However, we consider synneusis unlikely to be responsible for the greater abundance of twinning in the lower pressure sample compared to the higher pressure sample analyzed in this study, for three reasons:

(1) Textural analyses of crystals forming along the 1 MPa/h decompression path and conversion of two-dimensional shapes into three dimensions (e.g., Brugger and Hammer 2010b) are inconsistent with an evolution of crystal shapes from elongate to more blocky as expected by synneusis (Duchêne et al. 2008; Pupier et al. 2008). The crystal aspect ratios appear completely unrelated to quench pressure and thus the evolution along the decompression path.

(2) Synneusis requires the movement of crystals and it occurs during crystal settling or as a result of magma flowage (Ross 1957; Schwindinger and Anderson 1989; Schwindinger 1999; Nespolo and Ferraris 2004). There is no evidence of magma flow or crystal settling/floating in these samples (Brugger and Hammer 2010a). The distribution of crystals and their textures are homogeneous throughout each sample charge. Inter-crystal lattice orientations appear random, suggesting no alignment of grains. Thermal gradients driving convection, if present, are insufficient to modify the phase abundances and compositions throughout the charges, and thus unlikely to drive crystal “swimming.”

(3) Synneusis twins can only form in a medium that is sufficiently fluid to allow extensive differential movement of crystals (Ross 1957). Nearly all documented examples of synneusis are in basaltic magmas and occasionally in andesitic magmas (Vogt 1921; Ross 1957; Vance and Gilreath 1967; Vance 1969). In silicic samples with very low crystal fractions, such as the ones in this study (see Brugger and Hammer 2010a), the viscosity of the suspension is determined almost entirely by the viscosity of the interstitial liquid (Ryerson et al. 1988; Stevenson et al. 1996), which is calculated to be  $2.6 \times 10^4$  Pa s in the higher pressure sample and  $1.0 \times 10^7$  Pa s in the lower pressure sample (Giordano et al. 2008). Thus the viscosity of these samples is approximately two to five orders of magnitude higher than the basalts that have shown evidence of synneusis. High melt viscosity reduces the

number of times that crystals accidentally come into contact. If crystals are moving about in a melt due to external forces (i.e., the host magma is flowing), then crystals may occasionally come into random contact. However, even if there is a reduction in the free energy of the system afforded by a twin alignment of crystals, the energy barrier preventing spontaneous rotation of a crystal through highly viscous melt is implausibly high.

## IMPLICATIONS

Recognition of growth twinning in these synthetic plagioclase crystals has important implications for interpreting the growth history of natural crystals and the conditions under which they formed.

### Growth mechanism

Crystal growth rates are in part controlled by the removal of the latent heat of crystallization from the crystal melt boundary and the diffusion of crystal-forming atoms toward the boundary. At near-equilibrium conditions, these two processes are slower than the rate of atom attachment to the crystal face and the crystal growth mechanism is said to be “interface controlled.” The resulting crystals are typically planar-faceted, convex, and euhedral (Lofgren 1974; Kirkpatrick 1975). Under conditions of high effective undercooling and high supersaturation, the rate of atom attachment is faster than the diffusion of chemical constituents to the crystal-melt boundary and the growth mechanism is “diffusion controlled” (Lofgren 1974; Kirkpatrick 1975). Plagioclase crystals that arise from diffusion controlled growth display characteristic anhedral crystal morphologies such as embayments, internal hopper cavities, or swallowtail protrusions (Lofgren 1974; Corrigan 1982; Hammer and Rutherford 2002). When such anhedral morphologies are observed in volcanic rocks, the presumption is that they formed by diffusion controlled growth in an environment where a boundary layer of incompatible elements developed around the growing crystal, and protuberances on the corners and edges of the crystal penetrated through the boundary layer into melt that was richer in crystal-forming components (Lofgren 1974; Philpotts 1990; Hammer 2005, 2008).

Our results suggest that the presence of boundary layers are not required for the formation of swallowtail and hopper morphologies and melt inclusions, and these features do not necessarily denote diffusion controlled growth. Rather, these textures may form as a result of the high energy boundary between twins. We show that rapid growth during the incipient stages of crystallization commonly leads to growth twinning defects in the crystal structures of plagioclase. Diffusion controlled growth and twin defect formation both occur at conditions favoring rapid crystal growth at high undercooling. However, we suggest that the structural defects (twins) established very early in a feldspar crystal’s growth history, which may not require a compositional boundary layer to initiate, may go on to play an important role in controlling the crystal’s final morphology.

### Melt inclusions

Twin boundaries in sample 15-4 are associated with morphological defects such as swallowtails, irregular crystal terminations, embayments, and melt inclusions (Figs. 4b–4f). The

association between swallowtails and twins is recognized in olivine crystals (Faure et al. 2003). In addition, melt inclusions are documented as occurring preferentially along twin boundaries in plagioclase (Punin et al. 2009). Some studies attribute linear bands of melt inclusions to synneusis or agglomeration of crystals (Goldstein and Luth 2006; Renner et al. 2002) or as the result of new hopper crystal growth on an older preexisting crystal (Kohut and Nielsen 2004). However, the strong correlation between morphological defects and twin boundaries observed in this study suggests that the protrusions necessary for the formation of melt inclusions may be the direct result of the higher energy boundary between twins.

Twinning initially forms as a result of a high degree of undercooling, as described above. Once the twins are established they persist even after the degree of undercooling lessens, because of the high activation energy for subsolidus restructuring (Buerger 1945). The energy to attach a new growth unit that straddles a twin plane is greater than for a perfect crystal (Cahn 1954; Smith and Brown 1988). Thus, attachment across a twin plane leads to a smaller energy reduction than attachment on either side of a twin boundary. It follows that atoms preferentially attach to areas of the growing crystal that do not lie along the twin boundary. This leads to the formation of embayments, swallowtails, hopper crystals, and uneven crystal terminations (Punin et al. 2009), thus giving rise to the necessary precursors for the formation of melt inclusions (Roedder 1984; Kohut and Nielsen 2004; Faure and Schiano 2005).

#### ACKNOWLEDGMENTS

Thanks go to Scott Sitzman for setting up our EBSD system, teaching us how to use it, and answering countless questions. Additional thanks to Kazuhide Nagashima and Gary Huss for assistance with the SEM. This work was also improved through discussions with Benoît Welsch and reviews by Michael Zieg and Martin Streck. This work was supported by National Science Foundation CAREER award (EAR04-49888 to J.E.H.).

#### REFERENCES CITED

- Angel, R.J., Carpenter, M.A., and Finger, L.W. (1990) Structural variation associated with compositional variation and order-disorder behavior in anorthite-rich feldspars. *American Mineralogist*, 75, 150–162.
- Borg, I.Y., and Handin, J. (1966) Experimental deformation of crystalline rocks. *Tectonophysics*, 3, 249–368.
- Borg, I.Y., and Heard, H.C. (1969) Mechanical twinning and slip in experimentally deformed plagioclases. *Contributions to Mineralogy and Petrology*, 23, 128–135.
- Brugger, C.R., and Hammer, J.E. (2010a) Crystallization kinetics in continuous decompression experiments: Implications for interpreting natural magma ascent processes. *Journal of Petrology*, 51, 1941–1965.
- (2010b) Crystal size distribution analysis of plagioclase in experimentally decompressed hydrous rhyodacite magma. *Earth and Planetary Science Letters*, 300, 246–254.
- Buerger, M.J. (1945) The genesis of twin crystals. *American Mineralogist*, 30, 469–482.
- Cahn, R.W. (1954) Twinned crystals. *Advances in Physics*, 3, 202–445.
- Cashman, K.V. (1990) Textural constraints on the kinetics of crystallization of igneous rocks. *Reviews in Mineralogy*, 24, 259–314.
- (1992) Groundmass crystallization of Mount St. Helens dacite 1980–1986: a tool for interpreting shallow magmatic processes. *Contributions to Mineralogy and Petrology*, 109, 431–449.
- (1993) Relationship between plagioclase crystallization and cooling rate in basaltic melts. *Contributions to Mineralogy and Petrology*, 113, 126–142.
- Castro, J., Manga, M., and Cashman, K. (2002) Dynamics of obsidian flows inferred from microstructures: insights from microlite preferred orientations. *Earth and Planetary Science Letters*, 199, 211–226.
- Corrigan, G.M. (1982) The crystal morphology of plagioclase feldspar produced during isothermal supercooling and constant rate cooling experiments. *Mineralogical Magazine*, 46, 433–439.
- Deer, W.A., Howie, R.A., and Zussman, J. (1992) *An Introduction to the Rock-Forming Minerals*, 2<sup>nd</sup> edition, 407 p. Addison Wesley Longman, Hong Kong.
- Dowty, E. (1980) Computing and drawing crystal shapes. *American Mineralogist*, 65, 465–471.
- (2008) SHAPE. Version 7.2.3. Shape Software, Kingsport, Tennessee, U.S.A. <http://www.shapesoftware.com>.
- Duchêne, S., Pupier, E., Le Carlier de Veslud, C., and Toplis, M.J. (2008) A 3D reconstruction of plagioclase crystals in a synthetic basalt. *American Mineralogist*, 93, 893–901.
- Emmons, R.C., and Gates, R.M. (1943) Plagioclase twinning. *Bulletin of the Geological Society of America*, 54, 287–304.
- Faure, F., and Schiano, P. (2005) Experimental investigation of equilibration conditions during forsterite growth and melt inclusion formation. *Earth and Planetary Science Letters*, 236, 882–898.
- Faure, F., Trolliard, G., Nicollet, C., and Montel, J.-M. (2003) A developmental model of olivine morphology as a function of the cooling rate and the degree of undercooling. *Contributions to Mineralogy and Petrology*, 145, 251–263.
- Gaubert, P. (1896) Sur la production artificielle de la macle des spinelles dans les cristaux d'azotate de plomb. *Bulletin de la Société Française de Mineralogie*, 19, 431–434 (in French).
- Genareu, K., Valentine, G.A., Moore, G., and Hervig, R.L. (2010) Mechanisms for transition in eruptive style at a monogenetic scoria cone revealed by microtextural analyses (Lathrop Wells volcano, Nevada, U.S.A.). *Bulletin of Volcanology*, 72, 593–607.
- Geschwind, C.-H., and Rutherford, M.J. (1995) Crystallization of microlites during magma ascent: the fluid mechanics of 1980–1986 eruptions at Mount St. Helens. *Bulletin of Volcanology*, 57, 356–370.
- Giordano, D., Russell, J.K., and Dingwell, D.B. (2008) Viscosity of magmatic liquids: A model. *Earth and Planetary Science Letters*, 271, 123–134.
- Goldstein, S.B., and Luth, R.W. (2006) The importance of cooling regime in the formation of melt inclusions in olivine crystals in haplobasaltic melts. *The Canadian Mineralogist*, 44, 1543–1555.
- Hammer, J.E. (2005) Strange attractors: symbiosis in magma crystallization. *EOS Transactions, American Geophysical Union*, 86 (52), Fall Meeting Supplement, Abstract V12A-07. American Geophysical Union Fall Meeting, San Francisco, California.
- (2008) Experimental studies of the kinetics and energetics of magma crystallization. *Reviews in Mineralogy and Geochemistry*, 69, 9–59.
- (2009) Capturing crystal growth. *Geology*, 37, 1055–1056.
- Hammer, J.E., and Rutherford, M.J. (2002) An experimental study of the kinetics of decompression-induced crystallization in silicic melts. *Journal of Geophysical Research*, 107, 1–23.
- Hammer, J.E., Cashman, K.V., Hoblitt, R.P., and Newman, S. (1999) Degassing and microlite crystallization during pre-climatic events of the 1991 eruption of Mt. Pinatubo, Philippines. *Bulletin of Volcanology*, 60, 355–380.
- Hammer, J.E., Cashman, K.V., and Voight, B. (2000) Magmatic processes revealed by textural and compositional trends in Merapi dome lavas. *Journal of Volcanology and Geothermal Research*, 100, 165–192.
- Hammer, J.E., Sharp, T.G., and Wessel, P. (2010) Heterogeneous nucleation and epitaxial crystal growth of magmatic minerals. *Geology*, 38, 367–370.
- Higgins, M.D., and Chandrasekharan, D. (2007) Nature of sub-volcanic magma chambers, Deccan Province, India: evidence from quantitative textural analysis of plagioclase megacrysts in the Giant Plagioclase Basalts. *Journal of Petrology*, 48, 885–900.
- Ikeda, S., Toriumi, M., Yoshida, H., and Shimizu, I. (2002) Experimental study of the textural development of igneous rocks in the late stage of crystallization: the importance of interfacial energies under non-equilibrium conditions. *Contributions to Mineralogy and Petrology*, 142, 397–415.
- Johnsen, A. (1907) Tschermak's Zwillingstheorie und das Gesetz der Glimmerzwillinge. In M. Bauer, E. Koken, and Th. Liebisch, Eds., *Centralblatt für Mineralogie, Geologie und Paläontologie*, 400–409. Stuttgart (in German).
- Kelton, K.F. (2004) Nucleation in glasses and liquids and nanostructure formation. *Physics and Chemistry of Glasses, European Journal of Glass Science and Technology Part B*, 45, 64–70.
- Kirkpatrick, R.J. (1975) Crystal growth from a melt: A review. *American Mineralogist*, 60, 798–814.
- Kitazawa, S., Sunagawa, I., and Endo, Y. (1971) Growth and dissolution of cadmium iodide crystals. *Mineralogical Society of Japan Special Paper* 1, 109–113. *Proceedings IMA-IGAD Meetings '70*, IMA Volume.
- Kohut, E., and Nielsen, R.L. (2004) Melt inclusion formation mechanisms and compositional effects in high-An feldspar and high-Fo olivine in anhydrous mafic silicate liquids. *Contributions to Mineralogy and Petrology*, 147, 684–704.
- Larsen, J.F. (2006) Rhyodacite magma storage conditions prior to the 3430 yBP caldera-forming eruption of Aniakhak volcano, Alaska. *Contributions to Mineralogy and Petrology*, 152, 523–540.
- Lofgren, G.E. (1974) An experimental study of plagioclase crystal morphology: isothermal crystallization. *American Journal of Science*, 274, 243–273.
- Martel, C., and Poussineau, S. (2007) Diversity of eruptive styles inferred from the microlites of Mt Pelée andesite (Martinique, Lesser Antilles). *Journal of Volcanology and Geothermal Research*, 166, 233–254.

- Nespolo, M., and Ferraris, G. (2004) The oriented attachment mechanism in the formation of twins—A survey. *European Journal of Mineralogy*, 16, 401–406.
- Noguchi, S., Toramaru, A., and Shimano, T. (2006) Crystallization of microlites and degassing during magma ascent: Constraints on the fluid mechanical behavior of magma during the Tenjo eruption on Kozu Island, Japan. *Bulletin of Volcanology*, 68, 432–449.
- Noguchi, S., Toramaru, A., and Nakada, S. (2008) Relation between microlite textures and discharge rate during the 1991–1995 eruptions at Unzen, Japan. *Journal of Volcanology and Geothermal Research*, 175, 141–155.
- Ohfuji, H., Boyle, A.P., Prior, D.J., and Rickard, D. (2005) Structure of framboidal pyrite: An electron backscatter diffraction study. *American Mineralogist*, 90, 1693–1704.
- Philpotts, A.R. (1990) *Principles of Igneous and Metamorphic Petrology*, 498 p. Prentice Hall, New Jersey.
- Porter, D.A., and Easterling, K.E. (1992) *Phase Transformations in Metals and Alloys*, 2<sup>nd</sup> edition, 514 p. Chapman and Hall, London.
- Prior, D.J., Boyle, A.P., Brenker, F., Cheadle, M.C., Day, A., Lopez, G., Peruzzo, L., Potts, G.J., Reddy, S., Spiess, R., Timms, N.E., Trimby, P., Wheeler, J., and Zetterström, L. (1999) The application of electron backscatter diffraction and orientation contrast imaging in the SEM to textural problems in rocks. *American Mineralogist*, 84, 1741–1759.
- Prior, D.J., Mariani, E., and Wheeler, J. (2009) EBSD in the Earth Sciences: Applications, common practice, and challenges. In A.J. Schwartz, M. Kumar, B.L. Adams, and D.P. Field, Eds., *Electron Backscatter Diffraction in Materials Science*, 2<sup>nd</sup> ed., 345–360. Springer, New York.
- Punin, Y.O., Shtukenberg, A.G., Smetannikova, O.G., and Amelin, K.S. (2009) Plagioclase twin associations from the basic volcanic rocks of the Kamchatkan, Russia: Growth conditions and formation mechanisms. *European Journal of Mineralogy*, 22, 139–145.
- Pupier, E., Duchene, S., and Toplis, M.J. (2008) Experimental quantification of plagioclase crystal size distribution during cooling of basaltic liquid. *Contributions to Mineralogy and Petrology*, 155, 555–570.
- Renner, J., Evans, B., and Hirth, G. (2002) Grain growth and inclusion formation in partially molten carbonate rocks. *Contributions to Mineralogy and Petrology*, 142, 501–514.
- Roedder, E. (1984) Fluid Inclusions. *Reviews in Mineralogy and Geochemistry*, 12, 644 p.
- Ross, J.V. (1957) Combination twinning in plagioclase feldspars. *American Journal of Science*, 255, 650–655.
- Ryerson, F.J., Weed, H.C., and Piwinski, A.J. (1988) Rheology of subliquidus magmas I: picritic compositions. *Journal of Geophysical Research*, 93, 3421–3436.
- Schaskolsky, M., and Schubnikow, A. (1933) Über die künstliche Herstellung gesetzmässiger Kristallverwachsungen des Kalialauns. *Zeitschrift für Kristallographie*, 85, 1–16 (in German).
- Schiavi, F., Walte, N., and Kepler, H. (2009) First in situ observation of crystallization processes in a basaltic–andesitic melt with the moissanite cell. *Geology*, 37, 963–966.
- Schwindinger, K.R. (1999) Particle dynamics and aggregation of crystals in a magma chamber with application to Kilauea Iki olivines. *Journal of Volcanology and Geothermal Research*, 88, 209–238.
- Schwindinger, K.R., and Anderson, A.T. (1989) Synneusis of Kilauea Iki olivines. *Contributions to Mineralogy and Petrology*, 103, 187–198.
- Smith, J.V. (1974a) *Feldspar Minerals*, volume 1: Crystal Structure and Physical Properties, 627 p. Springer-Verlag, New York.
- (1974b) *Feldspar Minerals*, volume 2: Chemical and Textural Properties, 690 p. Springer-Verlag, New York.
- Smith, J.V., and Brown, W.L. (1988) *Feldspar Minerals*, volume 1: Crystal Structures, Physical, Chemical, and Microtextural Properties, 828 p. Springer-Verlag, New York.
- Stevenson, R.J., Dingwell, D.B., Webb, S.L., and Sharp, T.G. (1996) Viscosity of microlite-bearing rhyolitic obsidians: an experimental study. *Bulletin of Volcanology*, 58, 298–309.
- Spiess, R., Peruzzo, L., Prior, D.J., and Wheeler, J. (2001) Development of garnet porphyroblasts by multiple nucleation, coalescence and boundary misorientation-driven rotations. *Journal of Metamorphic Geology*, 19, 269–290.
- Sunagawa, I. (2005) *Crystals: Growth, morphology, and perfection*, 295 p. Cambridge University Press, New York.
- Vance, J.A. (1969) On synneusis. *Contributions to Mineralogy and Petrology*, 24, 7–29.
- Vance, J.A., and Gilreath, J.P. (1967) The effect of synneusis on phenocryst distribution patterns in some porphyritic igneous rocks. *American Mineralogist*, 52, 529–536.
- Vinet, N., and Higgins, M.D. (2010) Magma solidification processes beneath Kilauea Volcano, Hawaii: A quantitative textural and geochemical study of the 1969–1974 Mauna Ulu lavas. *Journal of Petrology*, 51, 1297–1332.
- Viola, C. (1902) Beitrag zur Zwillingsbildung. *Zeitschrift für Kristallographie*, 36, 234–244 (in German).
- Vogt, J.H.L. (1921) The physical chemistry of the crystallization and magmatic differentiation of igneous rocks. *The Journal of Geology*, 29, 318–350.
- Welsch, B., Faure, F., Famin, V., Baronnet, A., and Bachelery, P. (2013) Dendritic crystallization: A single process for all the textures of olivine in basalts? *Journal of Petrology*, 54, 539–574.

MANUSCRIPT RECEIVED NOVEMBER 17, 2013

MANUSCRIPT ACCEPTED AUGUST 6, 2014

MANUSCRIPT HANDLED BY JESSICA LARSEN